arXiv:cond-mat/0309599v1 [cond-mat.supr-con] 26 Sep 2003

Spectrum of Third Sound Cavity Modes on Superfluid ^{3}He Films

A. Vorontsov and J. A. Sauls

Department of Physics and Astronomy,
Northwestern University, Evanston, IL 60208, USA

We report theoretical calculations of the spectrum of third sound modes for a cylindrically symmetric film of superfluid ^{3}He, and compare these results with experimental data for the mode frequencies and amplitude spectrum of surface waves of superfluid ^{3}He films.
PACS numbers: 67.57.-z,67.40.Hf,67.57.Dc

1. INTRODUCTION

Third sound is an oscillation of the superfluid component in the plane of the film, with the normal component clamped by viscosity to the substrate that supports the film. This sound mode was first discussed theoretically by Atkins for superfluid ^{4}He films in the context of the two-fluid model.[1] The oscillations of the superfluid component cause the level of the film to locally rise and fall (Fig. 1). The restoring force that stabilizes the oscillations is the van der Waals attraction between the helium and the substrate. The possibility of observing third sound in superfluid ^{3}He films was discussed by Eggenkamp et al.,[2] and the first experimental report of surface modes identified as third sound was by Schechter et al.[3] Here we report theoretical calculations of the spectrum of cavity modes of third sound in superfluid ^{3}He films with cylindrical symmetry and compare the results with the observed spectra.

2. CAVITY MODES

We consider ^{3}He films with thicknesses of order $d \simeq 300 - 400\,\mathrm{nm}$, roughly $3 - 6$ coherence lengths at zero pressure. These are thin films in

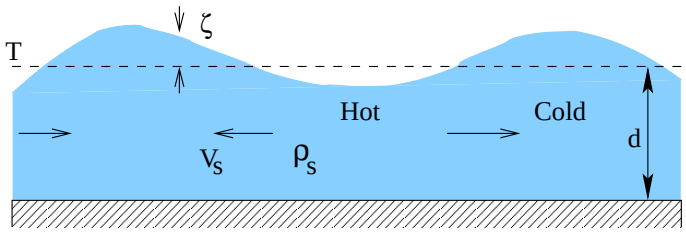


Fig. 1. Third sound oscillations of the superfluid produce surface waves.

the sense that they are expected to be in the either the axial or planar phase.[4] In either case the orbital anisotropy axis, $\boldsymbol{\ell}$, is anchored normal to the substrate. The analysis reported here assumes that the $\boldsymbol{\ell}$ vector remains fixed in the presence of small oscillations of the surface. We expect this to be a good approximation for long-wavelength, low-frequency third sound, since the coupling of the low-frequency normal-flapping mode in ^{3}He-A to transverse currents vanishes in the limit of exact particle-hole symmetry.[5] We also neglect edge currents associated with the broken chiral symmetry of ^{3}He-A, which may play an important role in nearly two-dimensional films with specular surfaces, but are not relevant for third sound in the geometry considered here.[6] Thus, in zero magnetic field the hydrodynamics of the superfluid film is defined by the phase mode and the surface excitation of the film, and reduces to scalar hydrodynamics. At temperatures $T \sim$ mK the viscous penetration depth is of order $\delta = \sqrt{2\eta/\rho\omega} \approx 1\,\mathrm{cm} \gg d$, for low frequency third sound ($\nu \sim 1\,\mathrm{Hz}$) (η and ρ are the viscosity and density of normal ^{3}He), and so we can safely consider the excitations (normal component) to be viscously clamped to the substrate. Furthermore, for third sound, the motion of the condensate is incompressible and confined to the plane of the film. Oscillations of the condensate then lead to height oscillations of the film. The hydrodynamic equations governing the excitation of the film include the continuity equation for mass conservation,

$$\rho \frac{\partial \zeta}{\partial t} + \rho_s d\, \boldsymbol{\nabla} \cdot \mathbf{v}_s = 0\,, \tag{1}$$

where ρ is the mass density, ζ is the deviation of the film height from its equilibrium value, d, and ρ_s is the superfluid density averaged over the thickness of the film. The pair momentum, or superfluid velocity, related to the phase ϑ of the condensate's wave function, $\mathbf{p}_s = \frac{\hbar}{2}\boldsymbol{\nabla}\vartheta = m_3 \mathbf{v}_s$, describes the in-plane motion of the condensate and obeys the Josephson equation of motion,

$$\frac{\partial \mathbf{v}_s}{\partial t} = -\boldsymbol{\nabla}\mu = -f\boldsymbol{\nabla}\zeta + s_f \boldsymbol{\nabla} T\,, \tag{2}$$

where μ is the chemical potential, f is the van der Waals force per unit mass, s_f is the entropy per unit mass and T is the absolute temperature. The oscillations of the condensate are coupled to entropy oscillations, and thus the height oscillations of third sound are coupled to the heat current in the film. This coupling, described by the heat transport equation,

$$\rho c_f d\frac{\partial T}{\partial t} + \rho s_f T\frac{\partial \zeta}{\partial t} - d\kappa_f \boldsymbol{\nabla}^2 T = 0\,, \tag{3}$$

where c_f is the specific heat and κ_f is the thermal conductivity per unit mass, is a key mechanism for damping of third sound cavity modes.

If we neglect heat transport in the film, then the height deviation, ζ, and the superfluid velocity, $\mathbf{v}_s$, obey two-dimensional wave equations with the phase velocity given by $c = \sqrt{\rho_s(T)df/\rho}$. For cylindrically symmetric films the eigenfunctions are products of Bessel functions (regular at $r = 0$) and azimuthal harmonics, $J_m(kr)\,e^{im\phi}$, where $k = \omega/c$ is the wavevector for the mode and $m = 0, \pm1, \pm2, \ldots$. The cavity mode eigenfrequencies are determined by the boundary conditions at the edge ($r = R$) of the film. For fixed boundary conditions, $\zeta(R) = 0$, the resonant frequencies and wavevectors are $\omega_{mn} = c(T)\,a_{mn}/R$, where a_{mn} is the $n^{\rm th}$ zero of $J_m(x)$. For free boundary conditions, $\partial_r\zeta(R) = 0$, $\omega_{mn} = c(T)\,a'_{mn}/R$, where (a'_{mn}) are the zeroes of the derivative, $J'_m(x)$. The general solution to the wave equation can then be expressed as an eigenmode expansion,

$$\zeta(r,\phi,t) = \sum_{m,n} A_{mn}\; J_m(\omega_{mn}r/c)\,e^{im\phi}\; e^{-i\omega_{mn}\,t}\,, \tag{4}$$

where the amplitudes, A_{mn}, are determined by driving forces that couple to the displacement.

3. ANALYSIS

Schechter et al.[3] observed standing waves of third sound on a circular substrate by exciting the surface with an a.c. electric field normal to the film. As noted in Ref. 7 the modes for thicker films ($250 - 400$ nm) are reasonably well indexed by assuming fixed boundary conditions, whereas thinner films ($d < 250$ nm) are better indexed assuming a free boundary condition. The mode frequencies for a 250 nm thick film are shown in Fig. 2. The temperature dependence reflects that of the superfluid density, which is approximately described by the Ginzburg-Landau form, $\rho_s(T)/\rho \propto 1 - T/T_c^{\rm film}$. The fit of the theoretical mode frequencies to the experimental data is done assuming that only the lowest frequency modes with $m = 0, 1$ are

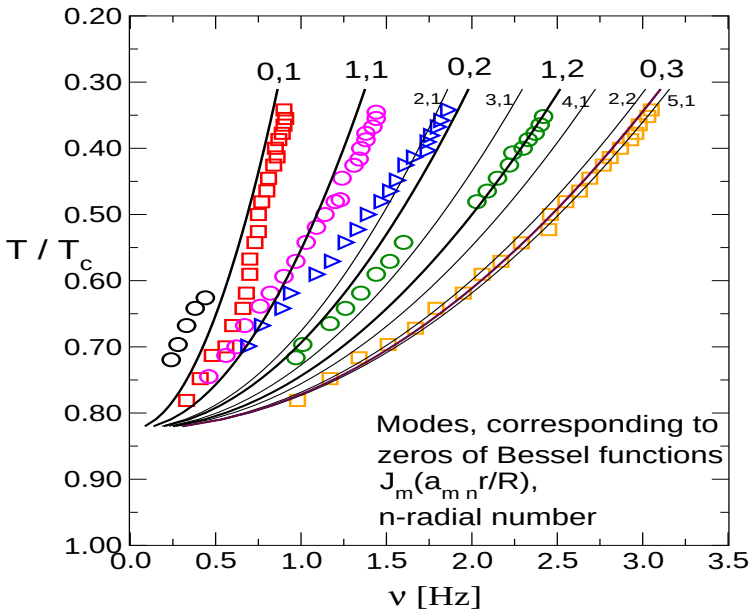


Fig. 2. Mode frequencies for a 250 nm film (symbols) from Ref. 7. The solid curves are the calculated mode frequencies with mode indices as labelled for fixed boundary conditions.

detected. In general there are higher frequency modes that may contribute, as well as modes with $m \geq 2$; these modes are also shown in Fig. 2 for comparison. It is not *apriori* obvious that these modes can be ignored. There are significant differences between theory and experiment, particularly for the lowest order modes. In order to more precisely identify the modes and to test the hydrodynamic theory for third sound oscillations of ^{3}He we have calculated the amplitude response of the film. The calculation includes the sensitivity of the detector for the various modes, and provides a determination of the amount of energy that is pumped into each mode.

The excitation field, or driving force, enters via the electrostatic energy density of the thin film which is a weak dielectric. The electro-chemical potential is then

$$\mu = \mu_0(T,\rho) - \frac{\mathbf{E}^2}{8\pi}\frac{\epsilon - 1}{\rho}\,, \tag{5}$$

where ρ is the mass density, ϵ is the dielectric constant of the liquid ^{3}He and $\mathbf{E}$ is the electric field. The response of the film to an a.c. voltage, $V(t) = V_0 + V_1 e^{i\omega t}$, is governed by the wave equation with the driving force

on the right-hand side,

$$\frac{\partial^2\zeta}{\partial t^2} - c^2\nabla^2\zeta = -c^2(T)\,A\sum_{m,n} f_{mn}J_m(a_{mn}\frac{r}{R})\cos(m\phi)\left(\frac{2V_1}{V_0}\right)e^{i\omega\,t} \qquad (6)$$

where $A \sim 2$Å is of the order of the surface wave amplitude and f_{mn} is the strength of the excitation force for mode (m,n). The capacitive excitation ring is displaced above the film and is slightly tilted about an axis (y-axis) the horizontal plane of the film.[3] If we measure the azimuthal angle with respect to the orthogonal direction in the plane (x-axis) then the resulting forces on the film are symmetric with respect to $\phi \to -\phi$. The surface displacement is then

$$\zeta(r,\phi,t) = A\left(\frac{2V_1}{V_0}\right)c^2\sum_{m,n}\frac{f_{mn}}{\omega_{mn}^2-\omega^2}J_m(a_{mn}r/R)\cos(m\phi)\,e^{i\omega\,t}\,. \qquad (7)$$

The capacitive detection method used in Refs. 3,7 allows one to measure the average displacement of the film surface. The amplitude spectrum, $A(\omega)$, is proportional to the average displacement and is given by

$$A(\omega) = A\left(\frac{2V_1}{V_0}\right)c^2(T)\left|\sum_{m,n}\frac{F_{mn}}{\omega_{mn}^2-\omega^2}\right|, \qquad (8)$$

where F_{mn} is the product of the excitation force (f_{mn}) and the detector sensitivity (D_{mn}) for mode (m,n): $F_{mn} = f_{mn} \times D_{mn}$. The detector sensitivity is determined by the electric field distribution for the geometry of the capacitor, which we calculate for the experimental setup of Ref. 3. The modes shown in Fig. 3 for the response are indeed the $m = 0, 1$ modes, which justifies the earlier assumption. However, the spectra shown in Fig. 3 differ significantly from the experimental spectra. There are many more modes visible in the calculated spectrum. This is a consequence of the assumption of frequency independent damping for the modes; constant damping does not suppress the higher frequency modes.

In general the damping of third sound is frequency dependent. In the following we calculate the frequency dependent damping rate for third sound that results from heat transport induced by the oscillations of the entropy associated with oscillations of the condensate. The resulting amplitude spectrum is obtained by replacing $\omega \to \omega + i\Gamma(T,\omega)$ in Eq. 8 in the response formula. The damping rate contains two terms, $\Gamma = \Gamma_0 + \Gamma_1(T,\omega)$, where Γ_0 is a constant damping rate which we attribute to roughness of the substrate and $\Gamma_1(\omega,T)$ is the damping obtained from the heat transport equation (Eq. 3),

$$\Gamma_1(\omega,T) = \frac{1}{2}\left(\frac{s_f}{c_f}\right)^2\frac{T\kappa_f(T)}{fd\rho c^2(T)}\,\omega^2 \equiv \Gamma_1\cdot\frac{t^2}{1-t}\,\omega^2\,, \qquad (9)$$

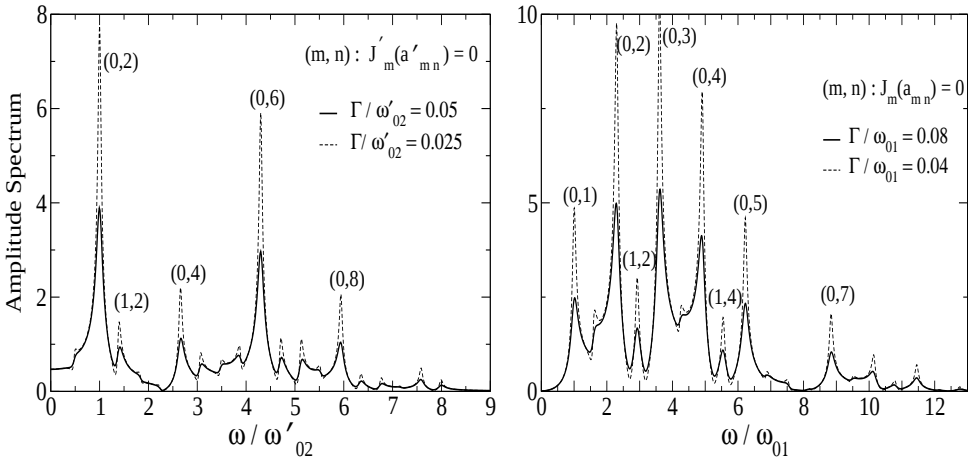


Fig. 3. Spectral weight for various modes of third sound folded with the detector sensitivity. The spectra are calculated assuming a constant, frequency independent damping, Γ, with free boundary conditions (left) and fixed boundary conditions (right).

where $t = T/T_c^{\rm film}$. Note that the damping rate diverges for $T \to T_c^{\rm film}$ because the superfluid stiffness vanishes whereas the thermal conductivity is finite. We have also assumed that surface pair breaking yields superfluidity with a gapless spectrum, in which case $s_f = c_f \approx \gamma_s T$ and $\kappa_f \propto T$.[4] The resulting damping rate leads to strong suppression of the higher frequency modes and much closer agreement with the experimental spectra. The calculated results for the amplitude spectra with both fixed and free boundary conditions are shown in comparison with the experimental spectra in Figs. 4 and 5. For the thick film with $d = 380\,\text{nm}$ the theoretically calculated spectrum are in reasonable agreement with the experimental spectrum for temperatures $T \lesssim 0.64\,\text{mK}$. At higher temperatures mixing or crossing of the modes is seen in the experimental spectrum. Such features are not observed in the theoretical spectra obtained for either type of boundary condition. The discrepancies are more severe for thinner films. In this case neither boundary condition yields agreement between the calculated and observed spectra. Experimentally, there is a much richer mode structure than the theoretically predicted spectrum.

4. CONCLUSIONS

In summary, the thicker films (250-400 nm) at low temperatures are reasonably well described by the equations of two-fluid hydrodynamics with

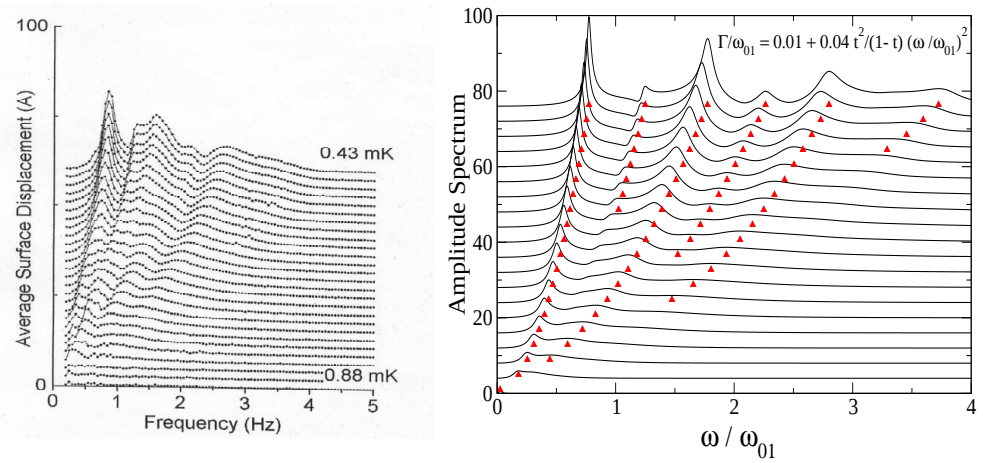


Fig. 4. Experimental spectra from Ref. 7 for a "thick" film with $d = 380$ nm (left) and the corresponding theoretical spectra calculated for fixed boundary conditions. Spectra for different temperatures are shifted vertically as indicated in the experimental figure.

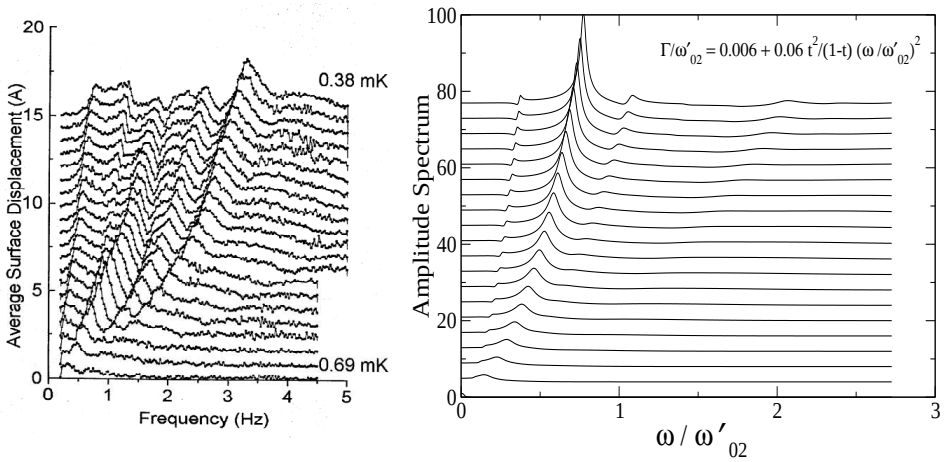


Fig. 5. Experimental spectra from Ref. 7 for a "thin" film (230 nm) and the corresponding theoretical spectra calculated with free boundary conditions.

damping due to surface roughness and thermal transport. The latter mechanism suppresses the higher frequency modes and diverges for $T \to T_c^{\rm film}$. In this regime the theoretically predicted modes and their spectral weights correspond to those observed in the experiment. The apparent mode splitting or mixing that onsets at higher temperatures, $T \gtrsim 0.65 T_c^{\rm film}$, may indicate a cross-over to a another mechanism for dissipation or, what seems more likely given the abruptness of the onset, a phase transition of the superfluid phase of the film. For thinner films (170-250 nm) we are not able to describe the observed spectra using two-fluid hydrodynamics with either set of boundary conditions and the same damping mechanisms. Although the frequencies of the modes can be associated with modes calculated with free boundary conditions, the spectral weights for the modes calculated from the theory do not agree with experiment. This fact, and mixing or splitting observed in thicker films may indicate that there is a phase transition at temperatures well below T_c for films with $d \sim 3 - 6\,\xi_0$.

ACKNOWLEDGEMENTS

We would like to thank A. Schechter for making his thesis available to us. This research was supported by NSF grant DMR-9972087.

REFERENCES

1. K. R. Atkins, *Phys. Rev.***113**, 962 (1959).
2. M. E. W. Eggenkamp, V. A. Shvartz, R. Blaauwgeers, A. Storm, R. Jochemsen, G. Frossati, *J. Low Temp. Phys.* **110**, 299 (1998).
3. A. Schechter, R. W. Simmonds, R. E. Packard, J. C. Davis, *Nature* **396**, 554 (1998).
4. A. Vorontsov, J. Sauls, *Phys. Rev. B* **68**, 064508 (2003).
5. S. K. Yip, J. A. Sauls, *J. Low Temp. Phys.* **86**, 257 (1992).
6. G. E. Volovik, *Sov. Phys. JETP*, **67**, 1804 (1992).
7. A. M. R. Schechter, Ph.D. thesis, University of California, Berkeley (1999).